Microchimica Acta (2020) 187:172
https://doi.org/10.1007/s00604-020-4143-9

ORIGINAL PAPER

Strand displacement-triggered G-quadruplex/rolling circle amplification strategy for the ultra-sensitive electrochemical sensing of exosomal microRNAs

Xiaoqi Tang[1] · Yang Wang[1,2] · Lin Zhou[1] · Wenqing Zhang[1] · Sha Yang[1] · Lianyu Yu[1] · Shuang Zhao[1] · Kai Chang[1] · Ming Chen[1,2,3]

Received: 27 December 2019 / Accepted: 24 January 2020

Abstract

Emerging evidence suggests that exosomal microRNAs are potential biomarkers for the early diagnosis and prognostic assessment of tumor. Here, we design a strand displacement-initiated G-quadruplex/rolling circle amplification (RCA) strategy for highly specific and sensitive electrochemical sensing of exosomal microRNAs. In the presence of exosomal miRNA-21, a locked nucleic acid (LNA)-labeled toehold mediated strand displacement reaction (TMSDR) is initiated, releasing output P2 to trigger the subsequent RCA reaction by hybridizing with the C-rich circular template. Then the obtained G-rich RCA products can bind to the probe anchored on the surface of gold electrode and generate G-quadruplex conformations. Based on the TMSDR-triggered G-quadruplex/RCA strategy, the detection limit of this electrochemical biosensor is down to 2.75 fM. Moreover, our biosensor exhibits excellent repeatability, stability, and high consistency compared to RT-PCR for clinical detection. In conclusion, this assay is expected to provide a hopeful strategy for the early non-invasive diagnosis and prognostic estimation of cancer.

Keywords Exosomal microRNAs · Locked nucleic acid · Strand displacement · Rolling circle amplification · G-quadruplex · Biosensor

Introduction

The liquid biopsy, a non-invasive means for tumor diagnosis, can be used to effectively track cancer development and explore the genetic landscape of tumor-linked lesions [1, 2]. Exosomal microRNAs, an important target of liquid biopsies, are intimately involved in the process of tumorigenesis, including cell proliferation, differentiation, and death [3, 4]. Compared to cell-free microRNAs, exosomal microRNAs possess distinctive advantages in terms of their quantity and stability in serum. This is probably attributable to the fact that exosomes can protect microRNAs from degradation by RNase and shear stress in the surrounding microenvironment [5]. In addition, exosomal microRNAs can directly reflect certain genetic properties of tumor cells [6]. Currently, exosomal microRNAs are considered potential biomarkers for the diagnosis and evaluation of breast cancer, lung cancer and ovarian cancer [7–9]. Therefore, the establishment of highly specific and sensitive technologies to detect exosomal microRNAs can improve the efficiency of early diagnosis, drug efficacy prediction, and prognostic assessment of several cancers.

At present, the most commonly used protocols for detecting exosomal microRNAs include reverse transcriptase PCR (RT-PCR), DNA microarrays, northern blotting [10–12].

Electronic supplementary material The online version of this article (https://doi.org/10.1007/s00604-020-4143-9) contains supplementary material, which is available to authorized users.

✉ Kai Chang
changkai0203@163.com

✉ Ming Chen
chming1971@126.com

[1] Department of Clinical Laboratory Medicine, Southwest Hospital, Third Military Medical University (Army Medical University), 30 Gaotanyan, Shapingba District, Chongqing 400038, China

[2] College of Pharmacy and Laboratory Medicine, Third Military Medical University (Army Medical University), 30 Gaotanyan, Shapingba District, Chongqing 400038, China

[3] State Key Laboratory of Trauma, Burn and Combined Injury, Third Military Medical University (Army Medical University), 30 Gaotanyan, Shapingba District, Chongqing 400038, China

However, these techniques are often time- and labor-consuming, have a high cost, and require complicated procedures, limiting their usefulness in biological and biomedical applications [13]. Biosensors, which are cost-effective, simple, and require lower sample volumes, show greater utility for clinical nucleic acid and protein detection [14, 15]. To successfully detect trace microRNAs, various biosensors have been fabricated based on different signal amplification strategies, such as rolling circle amplification (RCA), Y junction DNA probes, DNA walkers, and CRISPR [16–19]. Among these amplification strategies, RCA causes trace targets to produce high-molecular weight linear products to improve the magnifying power of the signal [20]. Importantly, RCA requires no labeling and has no specific temperature requirements [21], making it highly suitable for clinical practice [22]. As an improvement to this cascade signal amplification system, the RCA-assisted G-quadruplex conformation shows strong potential for the electrochemical sensing of exosomal microRNAs [23]. G-quadruplex [24, 25], as one of the most widely used DNAzymes [26], is formed by a G-rich DNA sequence with the participation of K^+ [27]. Moreover, it possesses efficient binding capacity with signal indicators such as methylene blue (MB) compared to double-stranded DNA due to end-stacking of the guanine quartet with a π-system to obtain the final desired signal strength [28]. Thus, the RCA-assisted G-quadruplex strategy is likely to dramatically improve signal amplification.

In addition, toehold mediate strand displacement reaction (TMSDR)-assisted magnetic bead separation technology may be useful for the specific detection of exosomal microRNAs. TMSDR, which is initiated by a short-overhang single-stranded region, can efficiently accomplish the specific identification of a target sequence at a constant temperature and displacement [29]. TMSDR has been used as a specific recognition strategy in the fabrication of various biosensors [30]. Moreover, the addition of locked nucleic acid (LNA), which contains a modified ribose moiety and is grossly similar to 2′-*O*-methyl RNA, can markedly enhance the melting temperature (Tm) differences between the base-mismatched sequence and the complementary duplex [31], further improving the specificity and accuracy of the system, even to the resolution of a single base [32]. Through the use of LNA-modified TMSDR, specific functional sequences are expected to be released to trigger a subsequent RCA reaction.

Herein, a highly specific and ultra-sensitive electrochemical biosensor for the exosomal microRNAs detection is presented, based on efficiently immobilizing signal indicator MB in a G-quadruplex conformation acquired by TMSDR-assisted RCA. This system is different from most current electrochemical sensors to detect microRNAs by capturing them on the surface of gold electrode (GE). Lightening the burden on electrode surface can be accomplished by establishing a target capture process in the liquid phase through the following process. First, the LNA-modified capture probe P1 is fixed on the magnetic beads and hybridized with the functional probe P2. When the target microRNA is isolated from exosomes, the LNA-modified P1 will capture it to stimulate the release of the functional probe P2 via TMSDR. Importantly, one end of P2 will generate substantial G-rich sequences via Phi29 DNA polymerase, while the other will hybridize with ssDNA to anchor the RCA products to the electrode. The RCA products are then incubated with K^+ and MB, and the signal indicator MB will embed the G-quadruplex units, which are made up of folded G-rich sequences, to produce a measurable electrochemical signal. Further, we attempted to validate this electrochemical biosensor in terms of its effectiveness, linearity, and stability through a series of tests and applications using miRNA-21 from breast cancer-derived exosomes. This biosensor may provide a promising strategy for the early non-invasive diagnosis, therapeutic monitoring, and prognostic estimation of tumor growth and development.

Materials and methods

Chemicals and reagents

Streptavidin-tagged magnetic beads (MNBs) were purchased from Bolanying Biotechnology Co., Ltd. (Chongqing, China). Phi29 DNA polymerase was obtained from New England Biolabs (Ipswich, MA, USA). Circular padlock, microRNAs, 20 bp DNA ladder and dNTPs (2.5 mM each) were purchased from Takara Bio (Shiga, Japan). 4-(2-hydroxyethyl)-1-piperazine ethanesulfonic acid sodium salt (HEPES) was obtained from Sangon Biotechnology Co., Ltd. (Shanghai, China). Tris(2-carboxyethyl) phosphine hydrochloride (TCEP, 98%), 6-mercapto-1-hexanol (MCH) and MB were acquired from Sigma Aldrich (St. Louis, MO, USA). Tween-20 and 5× TBE buffer were purchased from Solarbio Life Sciences (Beijing China). Super GelRed nuclear staining was acquired from Biotium (Fremont, CA, USA). Human serum samples were collected from Southwest Hospital in Chongqing, China. All custom-synthetic, HPLC-purified oligonucleotides (Table S1) employed in this work were purchased from Shanghai Sangon Biotechnology Co., Ltd. except microRNAs. Phosphate buffer solution (20 mM, pH 7.3) including 1 M NaCl, 1 mM EDTA, and 0.02% Tween-20 was used as coupling and storage buffer for MNBs. Tris-HCl buffer (10 mM, 100 mM NaCl, 1 mM EDTA, pH 7.4) served as the self-assembly buffer for ssDNA. MB was dissolved in 10 mM HEPES (pH 8.0) made up of 0.1 M KCl, and the electrochemical buffer was 20 mM HEPES (pH 8.0) including 20 mM KCl. All solutions were made with the ultrapure water (resistivity of 18.2 MΩ/cm) procured from the Millipore ultrapure water system.

Apparatus

Transmission electron microscopy (TEM) was conducted on the JEM-1400Plus electron microscope (JEOL Inc., Peabody, MA, USA). Fluorescence spectra was performed with F-7000 fluorescence spectrophotometer (Hitachi, Tokyo, Japan). RT-PCR was carried out with ABI 7500 Real-Time PCR machine (ABI, USA). Nanoparticle tracking analysis (NTA) was performed with the Zetasizer Nano ZSP (Malvern Instruments, Malvern, UK). Cyclic voltammetry (CV), electrochemical impedance spectroscopy (EIS) and differential pulse voltammetry (DPV) measurements were measured with the CHI760E electrochemical analyzer (Chenhua, Jiangsu, China).

Preparation of oligonucleotide-modified MNBs

According to the Bolanying's instructions, 80 μL streptavidin-modified MNBs (particle size: 1 μm; concentration: 20 mg/mL) were washed three times with 0.5 mL coupling buffer, then suspended in 0.5 mL coupling buffer including 8 μL of 100 μM LNA-tagged capture probe P1. After interacting with the tube rotator at ambient temperature for 0.5 h, the P1/MNBs were separated by a magnetic grate and washed three times with coupling buffer to remove excess P1. Next, 8 μL of 100 μM functional probe P2 was added to 492 μL P1/MNBs and incubated at room temperature overnight to form the P2/P1/MNBs complex, followed by washing three times to eliminate excess P2 in the supernatant. Finally, after separation by a magnetic grate, the P2/P1/MNBs solution was dispersed in 80 μL storage buffer and reserved at 4 °C for further use.

Capture of miRNA-21 and activation of RCA reaction

The indicated concentrations of target miRNA-21 or exosomal extract were added into 20 μL of the established P2/P1/MNBs solution, then diluted this mixture to 50 μL using coupling buffer. Subsequently, the solution was left for 1 h at room temperature to release the corresponding P2 from the MNBs through miRNA-21 induced TMSDR. P2 in the supernatant was accumulated and reserved at 4 °C after magnetic separation. And cy3-labeled P2 was utilized to optimize the concentration of P1. Briefly, after the same displacement process described above, the obtained supernatant was collected to measure the fluorescence at 550–650 nm with a certain excitation wavelength of 530 nm. The emission wavelength of 565 nm was employed to estimate the quantity of P2 release. Next, a solution containing 10 U Phi29 DNA polymerase, 2.5 mM dNTPs, 10 mM C-rich circular padlock, and bovine serum albumin was added to the supernatant to initiate the RCA reaction. The RCA reaction solution was then hatched at 30 °C for 2 h to generate many G-rich oligonucleotide sequences.

Fabrication of the biosensor and electrochemical measurements

The GE was burnished carefully with 0.3- and 0.05-μM alumina slurry and cleaned with ultrasonic in ethanol and ultrapure water for 2 min, respectively. After rinsing thoroughly and drying with ultrapure water and nitrogen gas flow, the GE was immersed in freshly prepared piranha solution (98% sulfuric acid and 30% hydrogen peroxide at a ratio of 3:1, *v*/v). After being rinsed and dried, the electrode was scanned by CV at 0–1.6 V in 0.5 M H_2SO_4 until the curve showed minimal fluctuations. The scan rate, quiet time, and sample interval were 0.1 V/s, 2 s, and 0.001 V, respectively. For functionalization of the GE, the ssDNA probe was modified with sulfhydryl group which could self-assemble on the GE surface by forming Au-S bond. 50 μL Tris-HCl (pH 7.4) including 1.5 μM ssDNA and 10 mM TCEP was incubated for 1 h to remove the disulfide bonds, followed by dropping 4 μL of the mixture onto the electrode surface and incubating at 37 °C overnight. The next day, after rinsed, the electrode was immersed in 1 mM MCH for 0.5 h to block any unoccupied binding sites and to eliminate any non-specifically absorbed ssDNA. Then, the RCA products were dropped onto the electrode surface and left at 37 °C for 2 h. Finally, each electrode was incubated with 4 μL of 10 mM HEPES containing 100 mM KCl and 1 mM MB at 37 °C for 2 h to allow the formation of MB/G-quadruplex structures. Final electrochemical signals were investigated by DPV in 20 mM HEPES (20 mM KCl, pH 8.0). The measuring parameters included: potential from −0.1 V to −0.6 V; amplitude: 0.01 V; pulse period: 100 ms; and pulse width: 50 ms. In addition, the entire process of sensor establishment was recorded by CV with the scan rate of 0.1 V/s ranging from −0.2 V to +0.6 V in 10 mM $[Fe(CN)_6]^{3-/4-}$ solution including 100 mM KCl. Likewise, EIS was executed in the same buffer with a frequency of $0.1–10^5$ Hz. All electrochemical detection protocols were performed with a classical three-electrode system composed of a platinum electrode, a saturated calomel electrode, and a GE described above.

Isolation of the exosomes

We collected the plasma from several patients suffering from breast cancer and pre-filtrated with a filter of pore size 0.45 μm. After pre-filtration, the plasma was centrifuged at 3000 rpm for 10 min at ambient temperature, and then at 16,000×*g* for 10 min at 4 °C. The pale yellow supernatant was collected, from which we extracted the exosomes in accordance with the manufacturer's instructions with use of exoEasy Maxi Kit (Qiagen, Hilden Germany).

Tem

The prepared exosomes were negatively stained with phosphortungstic acid (pH 6.5). Briefly, a carbon-coated copper grid was put on a 10-μL drop of exosomes for 10 min and dyed for 15 s. After removing the dye and drying at ambient temperature for 0.5 h, the sample was imaged using the JEM-1400Plus electron microscope.

Extraction and RT-PCR analysis of exosomal microRNAs

The exosomal microRNAs were extracted in accordance with the manufacturer's instructions with use of exoRNeasy Midi/Maxi Kit (Qiagen). Then, NanoPhotometer N50 (IMPLEN, Munich, Germany) was used to measure the quantitation of microRNAs.Total microRNAs were reverse transcribed to cDNA employing the miScript II RT Kit (Qiagen). The reaction mix was incubated at 37 °C for 60 min after adding the template microRNAs, followed by 95 °C for 5 min to inactivate the reverse transcriptase. Subsequently, RT-PCR was performed with the mix prepared by miScript SYBR Green PCR Kit (Qiagen) with the following thermal cycling states: 95 °C for 15 min; then continued 40 cycles of 94 °C for 15 s, 55 °C for 30 s, and 70 °C for 30 s.

Results and discussion

Design principle of the TMSDR-triggered G-quadruplex/RCA strategy

The experimental principle of this electrochemical biosensor is demonstrated in Scheme 1. Briefly, the TMSDR-triggered G-quadruplex/RCA strategy is as follows: the LNA-modified TMSDR is triggered by the presence of the target miRNA-21, and electrochemical detection is based on RCA-assisted G-quadruplex conformations. First, the LNA-modified capturre pobe P1 self-assembles onto the MNBs and hybridizes with the functional probe P2. When miRNA-21 is extracted from the exosomes derived from breast cancer patients, it will be recognized by the LNA-modified capture probe P1 to initiate the release of functional probe P2 via TMSDR. Notably, both ends of the free P2 play different roles in the subsequent reactions: one end is complementary to the C-rich RCA template, and the other is complementary to ssDNA to anchor the RCA products on the electrode surface. The released P2 remains in the supernatant after magnetic separation. Next, the C-rich circular template, Phi29 DNA polymerase, and dNTPs are added to the supernatant to trigger the RCA reaction and generate massive G-rich oligonucleotide sequences. The RCA products are then dropped onto the surface of the electrode to bind to ssDNA that was previously fixed on the electrode. Subsequently, through the activity of K^+, the free G-rich sequences can further fold into more G-quadruplex units to efficiently capture MB to substantially enhance the electrochemical peak current. The peak current will vary based on the concentration of released P2, proportional to the concentration of miRNA-21.

Exosomes characterization

The morphology of the purified exosomes derived from plasma of breast cancer patients was observed by TEM. As shown in Fig. 1A, the exosomes negatively stained with use of phosphotungstic acid had a representative saucer-like shape with a size of around 100 nm. And western blot was utilized to validate surface protein markers CD63 and CD9 of the exosomes [33]. As shown in Fig. 1B, the distinct bands further testified the properties of the isolated exosomes through comparing with the results of MCF-7 cells. The result of nanoparticle tracking analysis (NTA) verified the size distribution of isolated exosomes (Fig. 1C). The average size of the exosomes is around 192.7 nm.

Feasibility of the TMSDR-triggered G-quadruplex/RCA strategy

In order to validate the practicability of this electrochemical assay, we performed native PAGE and electrochemical characterization. As shown in Fig. 2A, P1 (lane 2) successfully combined with P2 (lane 3) to form a larger complex (lane 6). Furthermore, we verified that TMSDR was triggered to produce complexes between the target miRNA-21 and P1 with the release of P2 (lane 7). Lane 4 and lane 5 represented linear padlock and circular padlock, respectively. Lane 8 and lane 9 manifested the final results for the proposed assay without and with magnet-processed supernatant post addition of target miRNA-21, respectively. As expected, on the top of lane 9, the distinct band with extremely low mobility represented RCA products, confirming that RCA reaction was only triggered in the presence of the magnet-processed supernatant post addition of target miRNA-21. Additionally, the DPV peak currents were recorded with the modified electrode in different phases. As depicted in Fig. 2B, when ssDNA and MCH self-assembled on the bare GE successively, a DPV signal was observed, representing the nonspecific adsorption of MB (curve a). The DPV signal showed a negligible increase after the addition of RCA products in the absence of 1 nM miRNA-21 and Phi 29 DNA polymerase, respectively (curve b and c). However, after the addition of 1 nM miRNA-21, the electrode was incubated with the RCA products obtained by magnet-processed supernatant and Phi 29 DNA polymerase, and the DPV signal increased sharply (curve d).

The establishment of the electrochemical biosensor was also characterized by CV and EIS in 10 mM $[Fe(CN)_6]^{3-/4-}$

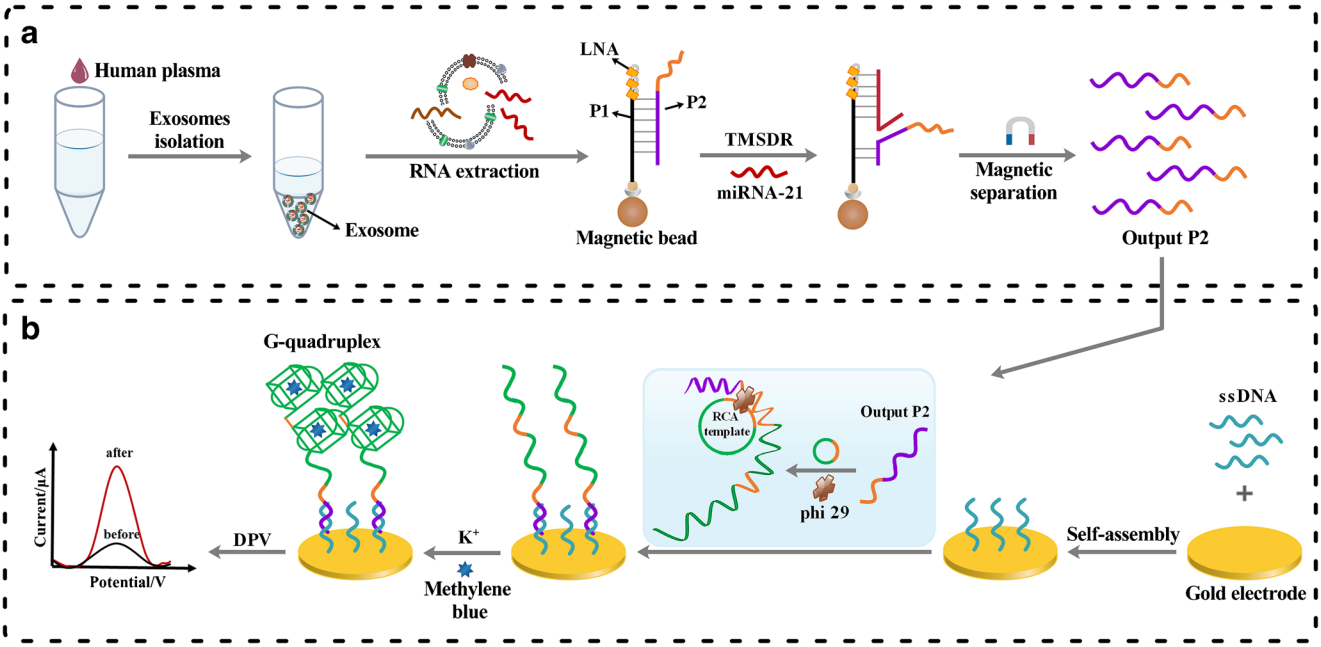

Scheme 1 Schematic illustration of the electrochemical sensing of exosomal miRNA-21: (A) Target capture mechanism and (B) construction of the proposed electrochemical biosensor.

with 100 mM KCl [34]. As depicted in Fig. 2C, we could observe a pair of redox peaks (curve a) for the bare GE. When the ssDNA and MCH were dropped onto the electrode surface in turn, the redox peaks decreased notably (curve b) due to the repulsion effect between the negatively charged phosphate backbone of ssDNA and $[Fe(CN)_6]^{3-/4-}$. Next,

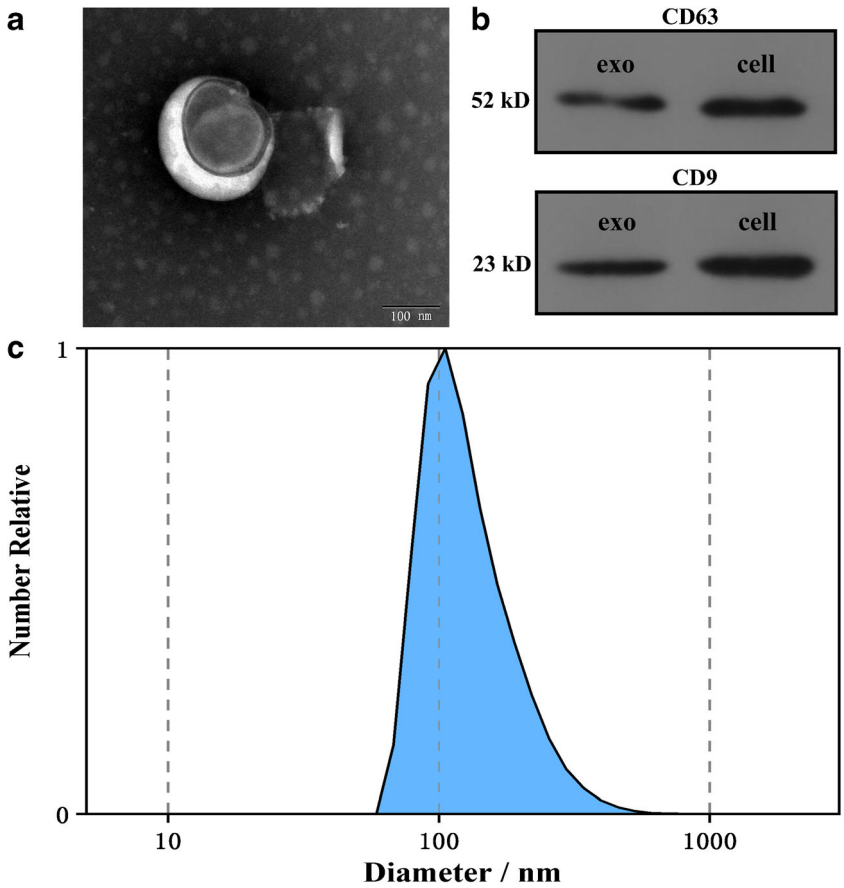

Fig. 1 Characterizations of the exosomes. (A) TEM image, (B) western blot analysis, and (C) nanoparticle tracking analysis (NTA) of the exosomes isolated from the plasma of breast cancer patients

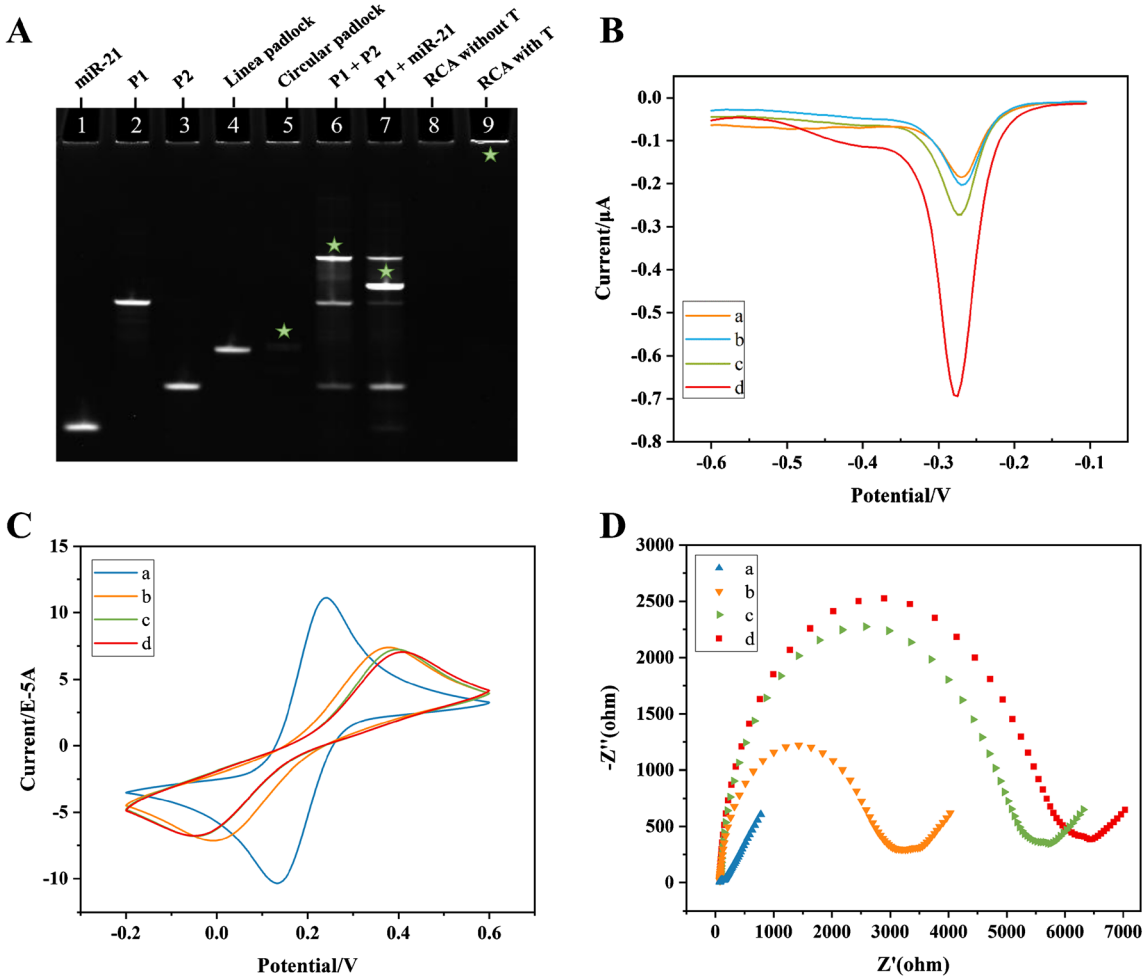

Fig. 2 (A) Native 12% PAGE gel analysis of the proposed electrochemical assay: Lane 1: miRNA-21, lane 2: P1, lane 3: P2, lane 4: linear padlock, lane 5: circular padlock, lane 6: P1 hybridized with P2 at 37 °C for 90 min, lane 7: lane 6 after hybridized with miRNA-21, lane 8 and lane 9 were the proposed assay without and with miRNA-21, respectively. (B) The DPV curves of the proposed electrochemical assay with different experiment conditions: (a) MCH-blocked ssDNA-modified gold electrode (GE), incubated with RCA products (b) without 1 nM miRNA-21, (c) without Phi 29 DNA polymerase and (d) both with 1 nM miRNA-21 and Phi 29 DNA polymerase. (C) The CV and (D) EIS curves of construction process of the GE surface: (a) bare GE, (b) MCH/ssDNA/GE, (c) RCA products/MCH/ssDNA/GE, (d) MB/RCA products/MCH/ssDNA/GE

upon the introduction of RCA products, the redox currents decreased slightly (curve c) due to the increase in biomolecules on the electrode surface. Subsequent incubation with K^+ and MB caused a further decrease in the redox peaks (curve d) by forming the MB/G-quadruplex structures.

Likewise, EIS showed a similar result to that of CV. Electron transfer resistance is known to directly reflect changes at the electrode interface [35]. As shown in Fig. 2D, the small semicircle diameter and the long tail denoting diffusion indicated the excellent conductivity of bare GE (curve a). Subsequent semicircles with increasing diameters indicated that the hindrance of electron transfer between the electrode and solution gradually increased after each step (curve b, curve c, curve d). These results verified that our designed electrochemical biosensor was successfully assembled.

Optimization of experimental conditions

Each experimental parameter may affect the correctness and effectiveness of our biosensor. Thus, to achieve optimal performance, several conditions that were most likely to affect the biosensor were optimized, including the concentration of P1, ssDNA, and K^+, as well as the RCA reaction time.

The first section of the assay determined the transformation efficiency of the target from P2. To study the effect of the concentration of P1 coupled to the MNBs, we analyzed the fluorescence intensity of released cy3-labeled P2 triggered by the target at different concentrations of P1 from 0.5–3.0 μM (Fig. 3A). The fluorescent signal reached an equilibration state at 1.5 μM P1. Thus, we chose 1.5 μM as the optimum concentration of P1 for maximum transformative capacity after capturing miRNA-21.

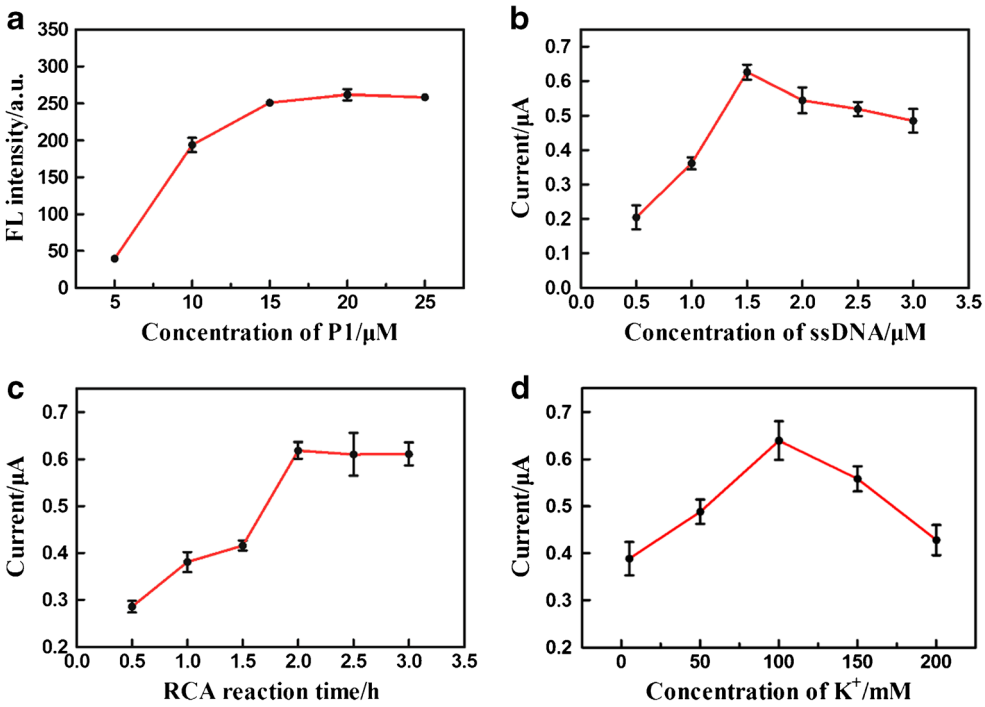

Fig. 3 Optimum conditions for this electrochemical biosensor. (A) The concentration of P1. (B) The concentration of ssDNA. (C) The RCA reaction time. (D) The concentration of K^+. Each point stands for the average value of five independent assays with error bars indicated

The density of ssDNA immobilized on the GE was modified by controlling the concentration of ssDNA dropped onto the GE surface. As shown in Fig. 3B, different concentrations of ssDNA ranging from 0.5–3.0 μM were added to the GE surface, incubated overnight, and tested by DPV. The maximum peak current was obtained at an ssDNA concentration of 1.5 μM. Conversely, the enhancement in concentration decreased the efficiency of subsequent hybridizations, suggesting that 1.5 μM was the optimum concentration of ssDNA.

To determine the influence of the RCA reaction time, the electrochemical biosensor was employed for detection with reaction times of 0.5–3 h. As presented in Fig. 3C, the signal response increased rapidly with increasing incubation time, but showed minimal changes at incubation times of longer than 2 h. Therefore, the optimum RCA reaction time was 2 h.

The final amplification of the electrochemical signal amplification largely depends on the effective formation of the G-quadruplex. Owing to its vital effect in the folding of G-quadruplex, the optimal concentration of K^+ is required to maximize the production of G-rich sequences to transform into the desired structures for binding the signal indicator MB. The electrochemical signal at different concentrations of K^+ was measured from 5 to 200 mM, as demonstrated in Fig. 3D. The maximum DPV value was observed at 100 mM, and the peak current decreased when the concentration was increased from 100 to 200 mM; thus, 100 mM was selected as the ideal concentration of K^+ for the miRNA-21 detection.

Performance of the proposed electrochemical biosensor

Under the above optimal conditions, we added diverse concentrations of miRNA-21 into the specific capture system containing MNBs and assessed by DPV. As exhibited in Fig. 4A, the peak current intensity of DPV gradually increased as the concentration of miRNA-21 increased. A good linear relationship was observed between the peak current of each response and the logarithm of the miRNA-21 concentration within a range of 10 fM to 10 nM with a correlation coefficient (R^2) of 0.9972. The linear fitting equation showed values of $I = 0.05687\log(C) + 0.2923$, where I and C stood for the peak current intensity and the concentration of target, respectively (Fig. 4B). The limit of detection (LOD) of this approach for miRNA-21 detection was calculated as 2.75 fM based on the rule of $3\sigma/k$ (in which the σ is the standard deviation of the blank signals and the k is the slope of the obtained linear fitting equation), that was lower than that of several previously published techniques for the detection of microRNAs (Table S2). This may be owing to the combination of the high amplification efficiency of the TMSDR-triggered G-quadruplex/ RCA strategy.

Selectivity of the proposed electrochemical biosensor

The specificity of the sensor is an important factor, as it is an indicator of its ability to discern only the molecule of interest. Consequently, several groups of similar molecules were utilized to verify the selectivity of the proposed sensor, including

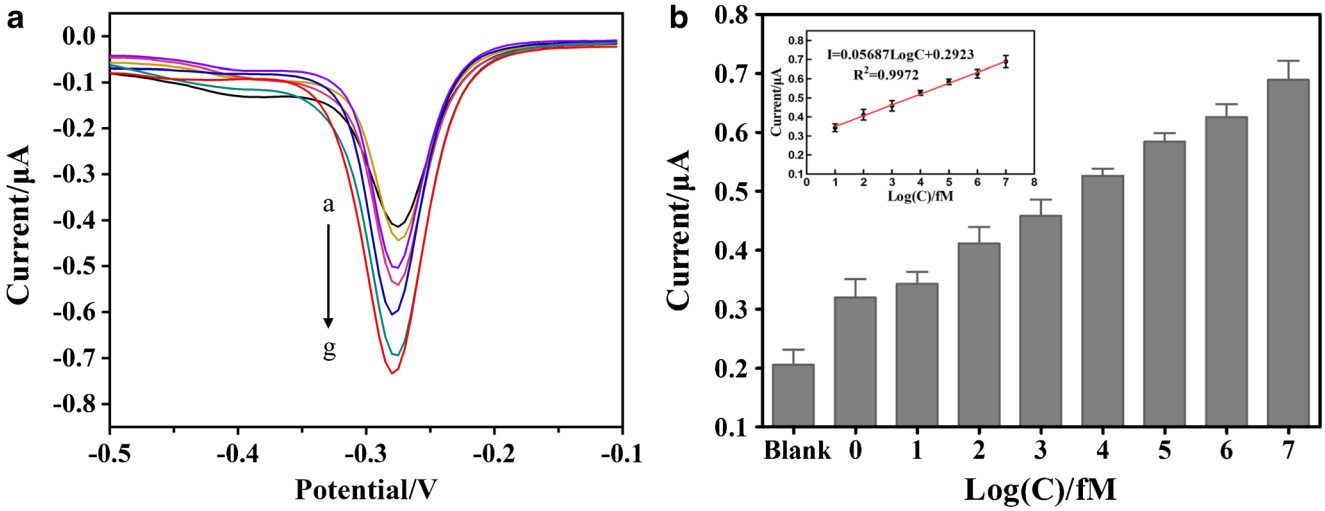

Fig. 4 (A) DPV signal for the electrochemical detection of miRNA-21. The concentration of miRNA-21 is (a) 10 fM, (b) 100 fM, (c) 1 pM, (d) 10 pM, (e) 100 pM, (f) 1 nM, (g) 10 nM. (B) The histogram of DPV current changes. The insert is the corresponding calibration plot for the DPV peak current vs Log(C)/fM. Each point stands for the average value of five independent assays with error bars indicated

Single base-mismatched target (SMT), two base-mismatched target (TMT), miRNA-145, miRNA-134, and miRNA-128. As shown in Fig. 5, the non-complementary targets miRNA-145, miRNA-134, and miRNA-128 induced an electrochemical signal that was indistinguishable from the blank signal. In addition, although the signals of TMT and SMT were slightly higher than blank signal, they remained significantly lower than the signal resulting from target binding. Thus, the proposed approach appeared to possess excellent specificity for target recognition, probably because of the high discriminative capacity of LNA.

Repeatability and stability of the proposed electrochemical biosensor

To explore the repeatability of this biosensor, identical electrodes were employed to detect miRNA-21 (1 pM) in ten successive tests, and the relative standard deviation (RSD) was 9.81%. This confirmed that the approach possesses excellent repeatability.

Additionally, we also assessed the stability of this biosensor. Three groups of identical electrodes modified with 1.5 μM ssDNA and 1 mM MCH were stored at 4 °C and incubated with 1 pM miRNA-21 every 7 days over 21 days. As depicted in Fig. S1, the DPV peak value of modified electrode was maintained at approximately 100.26% (day 7), 89.46% (day 14), and 78.01% (day 21) relative to the initial signal ($n = 3$), with an RSD of 6.31%, 0.25%, and 10.05%, respectively. This shows that the proposed electrochemical sensor possesses satisfactory stability.

Human serum analysis of exosomal miRNA-21

To verify the practicality of applying the proposed biosensor in a clinical environment, we compared the results of RT-PCR

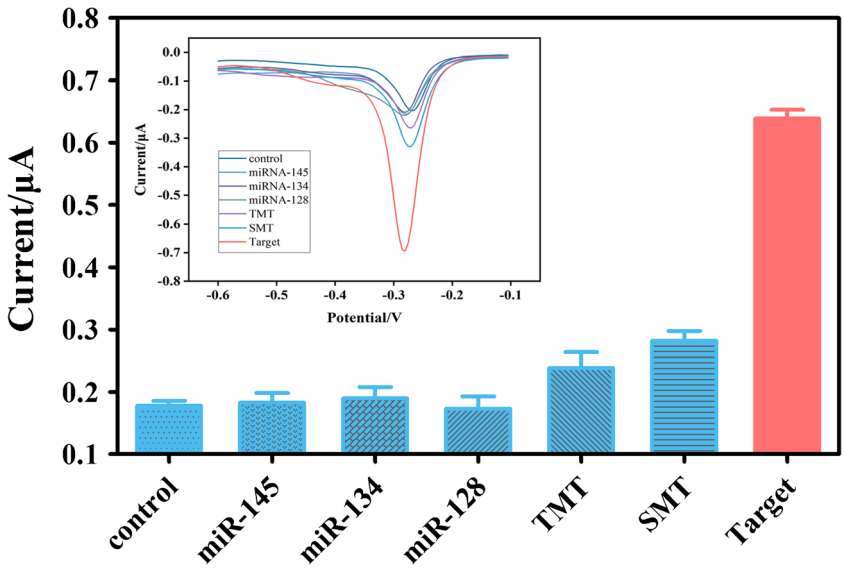

Fig. 5 Selectivity measurements toward: (a) Blank, (b) miRNA-145, (c) miRNA-134, (d) miRNA-128, (e) TMT, (f) SMT, (g) miRNA-21 at the same concentration (1 nM). Error bars represent standard deviations of three independent experiments. The insert is the DPV curves of each sample

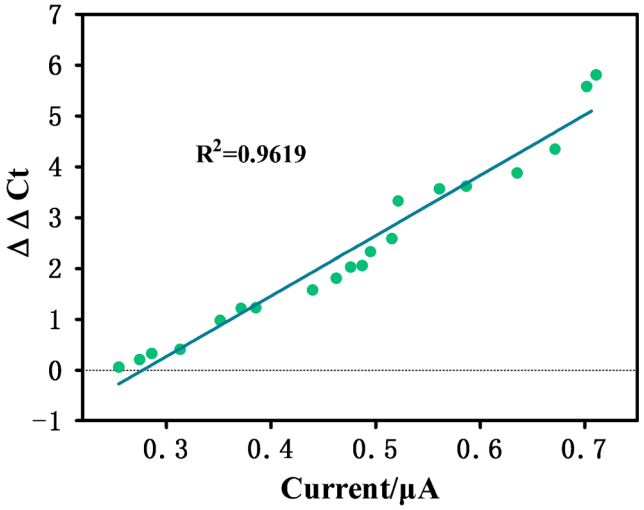

Fig. 6 Consistency between RT-PCR and the proposed electrochemical biosensor for the detection of exosomal miRNA-21 isolated from the plasma of breast cancer patients

with that of our biosensor by using both techniques to detect exosomal miRNA-21 from the plasma of breast cancer patients. All the template exosomal microRNAs were extracted from the same volume of plasma. In the RT-PCR reaction, the spiked miRNA-39 was used as the external control. After RT-PCR analysis, the Δ Δ threshold cycle (Δ Δ Ct) value of miRNA-21 was calculated by the Δ Ct value of the disease group subtracting the Δ Ct value of healthy group. Finally, the proposed electrochemical biosensor was employed to qualify the template exosomal miRNA-21. As shown in Fig. 6, we testified the consistency of two sets of data from RT-PCR and our biosensor by comparing the relative expression quantity (Δ Δ Ct) and DPV peak current of exosomal miRNA-21, respectively, in samples from breast cancer patients. It was found that the electrochemical results were in good accordance with the outcome of RT-PCR with a R^2 of 0.9619, verifying the clinical accuracy of this biosensor for exosomal miRNA-21 detection, which might provide a potential application in clinical diagnosis of cancer.

Conclusions

In summary, we successfully developed an electrochemical biosensor for the highly specific and sensitive detection of exosomal microRNAs based on strand displacement-triggered G-quadruplex/RCA signal amplification strategy. A specific LNA-modified DNA probe P1 was selected as the capture probe. The presence of target miRNA-21 could initiate strand displacement reaction and release the functional probe P2 which could further trigger RCA reaction by one end of P2 binding to the C-rich RCA template. Then a large number of G-rich RCA products could combine with the probe anchored on GE surface and lots of G-quadruplex conformations could be further generated with the participation of K^+. The RCA-assisted G-quadruplex conformation, in which the signal indicator MB could embed, was used as the detection probe. A cascade amplification electrochemical signal was produced by the integration of the RCA reaction and G-quadruplex structures. Under the optimum conditions, the proposed electrochemical biosensor responded linearly toward target miRNA-21 ranging from 10 fM to 10 nM with a detection limit of 2.75 fM. The biosensor had realized excellent specificity for miRNA-21 detection distinguished from base pair mismatch and other microRNAs. Furthermore, plasma obtained from breast cancer patients was collected to investigate the consistency between our designed biosensor and RT-PCR to verify its possibility of clinical application. Compared to several other previously reported detection methods (Table S2), the results shown here suggested that the proposed biosensor showed better detection limit and specificity. In conclusion, our electrochemical biosensor possesses major potential for the clinical detection of exosomal miRNA-21, and providing an improved strategy for the early diagnosis, therapeutic monitoring, and prognostic estimation of cancer.

Acknowledgements This work was supported by the National Natural Science Foundation of China (Grant No. 81430053, 81972027), Chongqing Health Commission (2018QNXM049, 2019ZDXM025) and Medical pre-research project of the Army Medical University (2018XYY04).

Compliance with ethical standards

Conflict of interest The author(s) declare that they have no competing interest.

References

1. Crowley E, Di Nicolantonio F, Loupakis F, Bardelli A (2013) Liquid biopsy: monitoring cancer-genetics in the blood. Nat Rev Clin Oncol 10:472–484
2. Sorbara L, Srivastava S (2019) Liquid biopsy: a holy grail for cancer detection. Biomark Med 13:991–994
3. Hannafon BN, Ding WQ (2013) Intercellular communication by exosome-derived microRNAs in cancer. Int J Mol Sci 14:14240–14269
4. He X, Ou C (2017) Exosome-derived microRNAs in cancer progression: angel or devil? J Thorac Dis 9:3440–3442
5. Tsui NB, Ng EK, Lo YM (2002) Stability of endogenous and added RNA in blood specimens, serum, and plasma. Clin Chem 48:1647–1653
6. Kosaka N, Iguchi H, Yoshioka Y, Takeshita F, Matsuki Y, Ochiya T (2010) Secretory mechanisms and intercellular transfer of microRNAs in living cells. J Biol Chem 285:17442–17452
7. Yoshikawa M, Iinuma H, Umemoto Y, Yanagisawa T, Matsumoto A, Jinno H (2018) Exosome-encapsulated microRNA-223-3p as a minimally invasive biomarker for the early detection of invasive breast cancer. Oncol Lett 15:9584–9592

8. Rabinowits G, Gercel-Taylor C, Day JM, Taylor DD, Kloecker GH (2009) Exosomal microRNA: a diagnostic marker for lung cancer. Clin Lung Cancer 10:42–46
9. Taylor DD, Gercel-Taylor C (2008) MicroRNA signatures of tumor-derived exosomes as diagnostic biomarkers of ovarian cancer. Gynecol Oncol 110:13–21
10. Thomou T, Mori MA, Dreyfuss JM, Konishi M, Sakaguchi M, Wolfrum C, Rao TN, Winnay JN, Garcia-Martin R, Grinspoon SK, Gorden P, Kahn CR (2017) Adipose-derived circulating miRNAs regulate gene expression in other tissues. Nature 542: 450–455
11. Ach RA, Wang H, Curry B (2008) Measuring microRNAs: comparisons of microarray and quantitative PCR measurements, and of different total RNA prep methods. BMC Biotechnol 8:69
12. Kim SW, Li Z, Moore PS, Monaghan AP, Chang Y, Nichols M, John B (2010) A sensitive non-radioactive northern blot method to detect small RNAs. Nucleic Acids Res 38:e98
13. Pritchard CC, Cheng HH, Tewari M (2012) MicroRNA profiling: approaches and considerations. Nat Rev Genet 13:358–369
14. Zhang X, Liu C, Pei Y, Song W, Zhang S (2019) Preparation of a novel Raman probe and its application in the detection of circulating tumor cells and Exosomes. ACS Appl Mater Interfaces 11: 28671–28680
15. Wang Y, Li Z, Liu M, Xu J, Hu D, Lin Y, Li J (2017) Multiple-targeted graphene-based nanocarrier for intracellular imaging of mRNAs. Anal Chim Acta 983:1–8
16. Li XY, Cui YX, Du YC, Tang AN, Kong DM (2019) Label-free telomerase detection in single cell using a Five-Base telomerase product-triggered exponential rolling circle amplification strategy. Acs Sensors 4:1090–1096
17. Zhou L, Wang Y, Yang C, Xu H, Luo J, Zhang W, Tang X, Yang S, Fu W, Chang K, Chen M (2019) A label-free electrochemical biosensor for microRNAs detection based on DNA nanomaterial by coupling with Y-shaped DNA structure and non-linear hybridization chain reaction. Biosens Bioelectron 126:657–663
18. Zhao L, Sun R, He P, Zhang X (2019) Ultrasensitive detection of Exosomes by target-triggered three-dimensional DNA walking machine and exonuclease III-assisted electrochemical Ratiometric biosensing. Anal Chem 91:14773–14779
19. Li Y, Teng X, Zhang K, Deng R, Li J (2019) RNA Strand displacement responsive CRISPR/Cas9 system for mRNA sensing. Anal Chem 91:3989–3996
20. Jiang HX, Liang ZZ, Ma YH, Kong DM, Hong ZY (2016) G-quadruplex fluorescent probe-mediated real-time rolling circle amplification strategy for highly sensitive microRNA detection. Anal Chim Acta 943:114–122
21. Deng R, Zhang K, Li J (2017) Isothermal amplification for MicroRNA detection: from the test tube to the cell. Acc Chem Res 50:1059–1068
22. Yi L, Qinli P, Junlong L, Lili Z, Yiyi T, Yuxia L, Wen Y, Guoming X (2017) An "off-on" fluorescent switch assay for microRNA using nonenzymatic ligation-rolling circle amplification. Mikrochim Acta 184:4323
23. Du YC, Zhu YJ, Li XY, Kong DM (2018) Amplified detection of genome-containing biological targets using terminal deoxynucleotidyl transferase-assisted rolling circle amplification. Chem Commun 54:682–685
24. Sen D, Gilbert W (1988) Formation of parallel four-stranded complexes by guanine-rich motifs in DNA and its implications for meiosis. Nature 334:364–366
25. Qian Y, Fan TT, Wang P, Zhang X, Luo JJ, Zhou FY, Yao Y, Liao XJ, Li YH, Gao FL (2017) A novel label-free homogeneous electrochemical immunosensor based on proximity hybridization-triggered isothermal exponential amplification induced G-quadruplex formation. Sensor Actuat B-Chem 248:187–194
26. Gao FL, Fan TT, Wu J, Liu S, Du Y, Yao Y, Zhou FY, Zhang Y, Liao XJ, Geng DQ (2017) Proximity hybridization triggered hemin/G-quadruplex formation for construction a label-free and signal-on electrochemical DNA sensor. Biosens Bioelectron 96:62–67
27. Zou R, Zhang F, Chen C, Cai C (2019) An ultrasensitive guanine wire-based resonance light scattering method using G-quadruplex self-assembly for determination of microRNA-122. Mikrochim Acta 186:599
28. Zhang FT, Nie J, Zhang DW, Chen JT, Zhou YL, Zhang XX (2014) Methylene blue as a G-quadruplex binding probe for label-free homogeneous electrochemical biosensing. Anal Chem 86:9489–9495
29. Srinivas N, Ouldridge TE, Sulc P, Schaeffer JM, Yurke B, Louis AA, Doye JP, Winfree E (2013) On the biophysics and kinetics of toehold-mediated DNA strand displacement. Nucleic Acids Res 41: 10641–10658
30. Li S, Liu X, Pang S, Lu R, Liu Y, Fan M, Jia Z, Bai H (2018) Voltammetric determination of DNA based on regulation of DNA strand displacement using an allosteric DNA toehold. Mikrochim Acta 185:433
31. Chen J, Zhang J, Wang K, Lin X, Huang L, Chen G (2008) Electrochemical biosensor for detection of BCR/ABL fusion gene using locked nucleic acids on 4-aminobenzenesulfonic acid-modified glassy carbon electrode. Anal Chem 80:8028–8034
32. Wegman DW, Ghasemi F, Stasheuski AS, Khorshidi A, Yang BB, Liu SK, Yousef GM, Krylov SN (2016) Achieving single-nucleotide specificity in direct quantitative analysis of multiple MicroRNAs (DQAMmiR). Anal Chem 88:2472–2477
33. Wen SW, Sceneay J, Lima LG, Wong CS, Becker M, Krumeich S, Lobb RJ, Castillo V, Wong KN, Ellis S, Parker BS, Moller A (2016) The biodistribution and immune suppressive effects of breast Cancer-derived Exosomes. Cancer Res 76:6816–6827
34. Yuan YH, Chi BZ, Wen SH, Liang RP, Li ZM, Qiu JD (2018) Ratiometric electrochemical assay for sensitive detecting microRNA based on dual-amplification mechanism of duplex-specific nuclease and hybridization chain reaction. Biosens Bioelectron 102:211–216
35. Patra S, Roy E, Madhuri R, Sharma PK (2015) Imprinted ZnO nanostructure-based electrochemical sensing of calcitonin: a clinical marker for medullary thyroid carcinoma. Anal Chim Acta 853: 271–284